Integrated Microwave and mm-Wave MIMO Antenna Module With 360° Pattern Diversity for 5G Internet of Things

Niamat Hussain, *Member, IEEE*, and Nam Kim

***Abstract*—The complete coverage of the operating frequency bands from microwave bands to millimeter (mm-wave) is required for the realization of the fifth-generation (5G) Internet of Thing (IoT) systems. Here, we present a multiband antenna operating at the microwave (2.5/3.5/5.5/7.5 GHz) and mm-wave bands (23–31 GHz), and its 12-port MIMO configuration with pattern diversity affording 360° coverage for 5G IoT applications. The multiband characteristics are obtained by adding well-designed quarter-wavelength stubs. The antenna operates at the important frequency bands from 2.37–2.65, 3.25–3.85, 5.0–6.1, and 7.15–8.5 GHz ($|S_{11}| < -10$ dB), while it resonates from 23–31 GHz at the mm-wave band with the desired radiation characteristics. Moreover, the antenna has more than 95% radiation efficiency and a stable gain (> 2.5 dBi at microwave band and 6.5 dBi at mm-wave bands) characteristics. In addition, the single-element antenna is translated to design a 2 × 2 MIMO antenna. This MIMO unit is further utilized in the formation of 2 × 4 and the proposed 3 × 4 (12-port) MIMO configurations to achieve spectral and pattern diversity. Considering the unique three-dimensional arrangement of the antenna elements, the 12-port MIMO system is the only one of its kind that offers the codesign of microwave and mm-wave antenna, good isolation, and pattern diversity, providing complete 360° space coverage in elevation and azimuth planes. The proposed antenna module is suitable for 5G IoT, especially in an indoor scenario for smart houses, offices, and vehicle-to-everything communications.**

***Index Terms*—Fifth-generation (5G) communication, Internet of Things (IoT) antenna, MIMO antenna, pattern diversity, sub-6 GHz and millimeter wave (mm-wave) antenna, vehicular communication.**

I. Introduction

THE COMBINATION of the fifth-generation (5G) communication and the Internet of Things (IoT) is going to wirelessly connect people, data, processes, infrastructure, and things around us with high data rates and low latency [1].

Manuscript received 14 June 2022; accepted 25 July 2022. Date of publication 28 July 2022; date of current version 7 December 2022. This work was supported in part by the Institute of Information and Communications Technology Planning and Evaluation (IITP) Grant funded by the Korean Government (MSIT, Development of Measured EMF Big Data Analysis and Management Platform) under Grant 2022-0-01031, and in part by the ICT Research and Development Program of MSIT/IITP (A Study on Public Health and Safety in a Complex EMF Environment) under Grant 2019-0-00102. *(Corresponding author: Nam Kim.)*

Niamat Hussain is with the Department of Smart Device Engineering, Sejong University, Seoul 05006, South Korea (e-mail: niamathussain@sejong.ac.kr).

Nam Kim is with the Department of Information and Communication Engineering, Chungbuk National University, Cheongju 28644, South Korea (e-mail: namkim@chungbuk.ac.kr).

Digital Object Identifier 10.1109/JIOT.2022.3194676

Fig. 1. Typical 5G network in a smart city.

The 5G-enabled IoT, along with artificial intelligence, will revolutionize the world by realizing smart cities, smart healthcare, smart farming, smart factories, intelligent transportation system (ITS), and augmented/virtual reality [2]. To ensure seamless connectivity, 5G technology uses two frequency bands: 1) the existing sub 6 GHz bands and 2) a new, unused spectrum of millimeter waves (mm-waves). This wide spectrum allows the 5G technology by supporting the high traffic growth and growing demand for high-bandwidth connectivity. A typical 5G network is shown in Fig. 1 [3]. The 4G and 5G macrocells working at sub-3 GHz and sub-6 GHz bands provide the essential wide coverage area, while the 5G small cells operating at mm-wave bands add ultimate capacity when needed.

Cisco Systems recently reported that 29.3 billion networked IoT devices will operate by 2023, outnumbering humans by more than threefold [4]. These devices and sensors use various frequency bands, for example, the scientific and medical band (ISM, 2.4 GHz), Bluetooth band (2.4 GHz), and long-term evolution band (LTE, 2.5 GHz), the 5G sub-6 GHz band (2.5/3.5 GHz), and the radio-frequency identification (RFID, 2.54/5.8 GHz), x-band (7–8 GHz), wireless local area network (WLAN, 2.4/5.2/5.8 GHz), downlink satellite communication (x-band, 7.36–8.06 GHz) band, and 5G mm-wave bands (24/26/28 GHz). The main challenge in the future IoT is reliable connectivity, which needs several frequency bands to avoid electromagnetic interference, energy efficiency to support continuous power to all devices, and the cost. This implies that antennas operating from sub-6 GHz to mm-waves are required for IoT communication. Various dedicated antennas for their applications in the IoT at sub-6 GHz and mm-wave bands have been widely studied in the literature [5]–[21]. These antennas operate either at sub-6 GHz [5]–[13] or mm-Wave bands [14]–[21]. Multiple antennas (operating at various frequencies) increase device size, cost, and complexity; new

5G devices must be small, inexpensive, and simple. To avoid this issue, shared aperture antennas have been investigated [22]–[24]. These kinds of antennas simply put two antennas together in a shared aperture, one for the sub-6 GHz band and the other for the mm-Wave bands. For example, the antennas presented in [25] and [26] operate both at 2.4/5.2 GHz and 60 GHz to integrate the existing Wi-Fi connection with the future high data rate Wi-Gig connections. The joint implementation of WLAN band and Wi-Gig can provide long- and short-range radio accesses with high-data simultaneously. Since most of the countries have adopted 2.5/3.5 and 24/26/28 GHz bands for their 5G communications. Therefore, multiband antennas have been designed at sub-6 GHz and mm-wave bands [27]–[33]. The Fabry-Perot cavity-based folded-parallel-plate antenna provides coverage for 2.4- and 28-GHz bands [27]. In [28], slots and patches are combined in a leaky-wave antenna to realize the dual-band function at 7 and 38 GHz. The aperture shared an array of dipole antennas that offer resonance at 3.5 and 28 GHz with stable radiation patterns [29]. A dielectric resonator slot antenna fed by a substrate-integrated waveguide operates at 5.2 and 24 GHz [30]. In [31], a dual function tampered slot structure is utilized to generate multiband characteristics at 2.5, 5.5, and 24/28 GHz. Furthermore, a planar antenna is presented using a mode-composite method [32]. In this design, a combination of a meander and an L-shaped SIW sections are used with multiple ports to obtain two bands at sub-6 GHz and two bands at mm-wave spectrum. Hussain [33] proposed a shared aperture square concentric slot-based 5G IoT antenna that operates simultaneously at various sub-6 GHz bands and 28-GHz bands. In the works mentioned earlier, the microwave antennas and mm-wave integrated antennas have been fed separately (at least two ports) at different points. This needs a lot of space for feed positions and a complex feeding network. The increased number of multiple ports restricts the MIMO configurations of these antenna designs, especially for the sub-6 GHz.

Recently, the problem of separately feeding the sub-6 GHz antenna and mm-wave antenna in the integrated shared aperture antennas has been addressed in [34], where a single-fed triple-band antenna operating at 3.5, 28, and 38 GHz and its MIMO configuration has been developed. This antenna has the advantages of single feed for both microwave and mm-wave antenna. In this design, the higher frequency patch is fed directly through a microstrip feedline, while the meander line is attached to the patch for its operation at 3.5 GHz. However, the antenna is specified for 5G phones; the 2.4-, 2.5-, 5.5-, and 7.5-GHz bands, which ensure 5G IoT connectivity is not covered.

Overall, it remains challenging to realize an integrated microwave and mm-wave MIMO antenna having the advantage of pattern diversity and necessary isolation for future IoT applications. Here, we present a single-fed multiband antenna working at the microwave (2.5/3.5/5.5/7.5 GHz) and mm-wave (24/26/28 GHz) bands and its 12-port MIMO configuration to provide connectivity for the 5G IoT devices and sensors. To our knowledge, the MIMO system is the first of its kind that has the ability to cover all the key bands with polarization diversity having low coupling among the MIMO elements for 5G-enabled IoT standards.

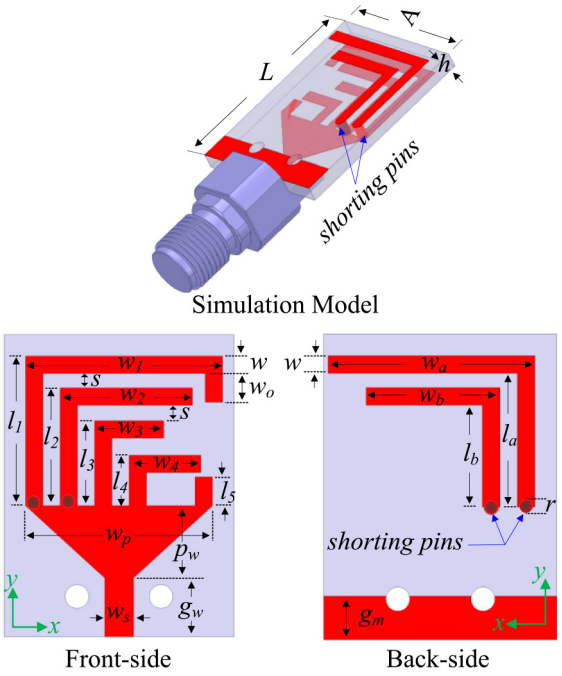

Fig. 2. Geometry of the integrated microwave and mm-wave antenna for 5G IoT applications.

II. Single-Element Antenna for 5G IoT Applications

The proposed multiband antenna operating at microwave and mm-wave bands for the 5G IoT application is discussed in this section. For easy understanding, the section is divided as follows.

A. Antenna Geometry

The configuration of the presented single-element antenna is shown in Fig. 2. The antenna consists of five metallic stubs connected to the triangular monopole at its front, while two stubs are connected to it at its backside through shoring vias. The antenna is designed on a high-frequency Rogers-5880 substrate ($\varepsilon_r = 2.2$, $\tan\delta = 0.0009$). The front metallic stubs act as quarter-wavelength monopoles to provide multiple resonances at 2.5, 3.5, 5.5, 7.5, and 28 GHz. At the same time, the stubs at the backside connected to the main radiator through shorting pins are employed for the bandwidth improvements at 2.5- and 3.5-GHz bands. The length of each stub is optimized to get resonances at microwave and mm-wave bands. The optimized parameters of the antenna are as follows: $A = 16$, $L = 21$, $h = 1.6$, $g_m = 3$, $w_s = 2$, $g_w = 4.1$, $w_p = 13$, $p_w = 5$, $l_1 = 10.5$, $w_1 = 13.7$, $l_2 = 8.2$, $w_2 = 9.2$, $l_3 = 5.9$, $w_3 = 4.8$, $l_4 = 3.5$, $w_4 = 5$, $l_5 = 2$, $s = 1$, $w = 1$, $w_o = 3.2$, $w_a = 14.2$, $w_b = 9.2$, $l_a = 10.5$, and $l_b = 8.2$ [unit = mm].

B. Design Procedure

The design commenced with a basic triangular monopole that featured a partial ground plane operating at a resonating

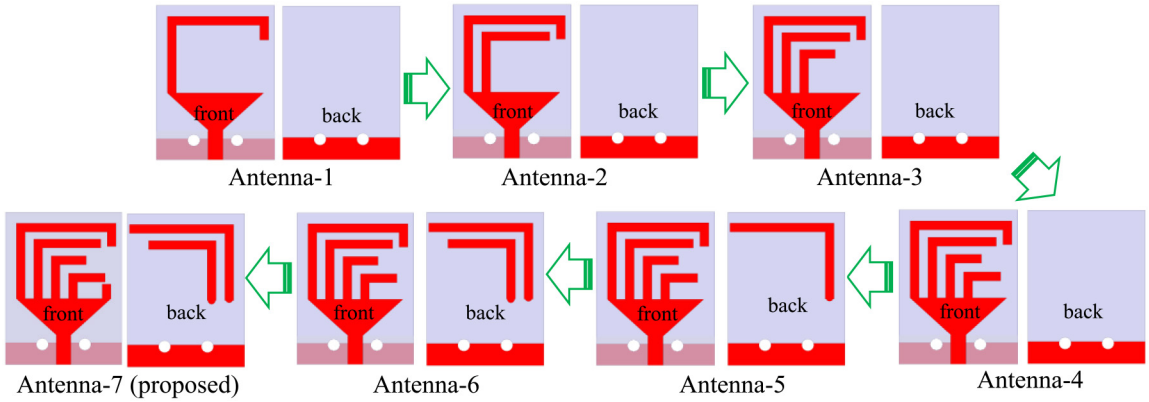

Fig. 3. Design procedure of the integrated microwave and mm-wave antenna for 5G IoT applications.

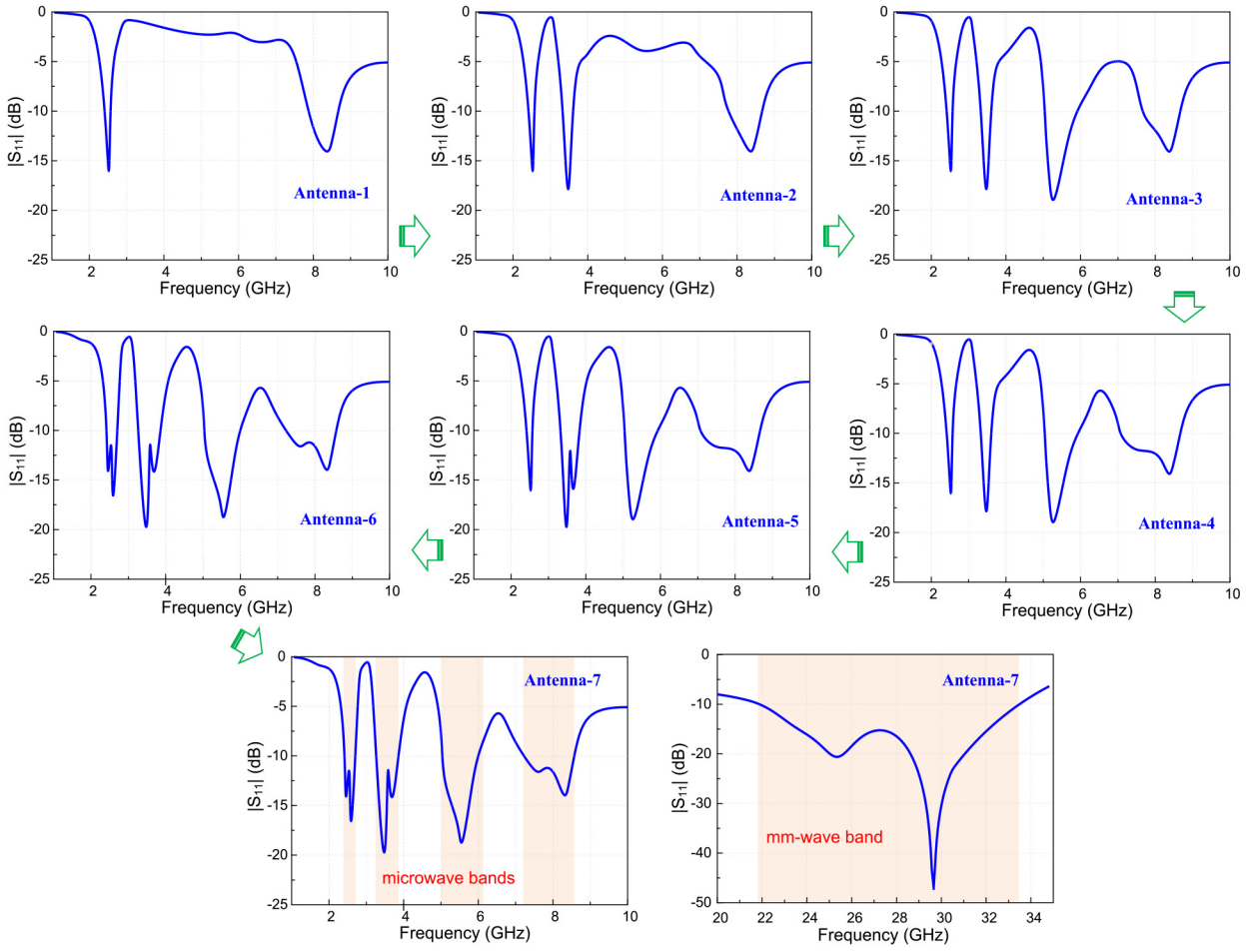

Fig. 4. $|S_{11}|$ of the proposed integrated microwave and mm-wave antenna for various design stages.

frequency (f_{res}) of 8.5 GHz. According to the theory of the transmission line model, the width (w_p) of the monopole can be approximated by

$$w_p \approx \frac{c}{4\, f_{\text{res}} \sqrt{\frac{\varepsilon_r+1}{2}}} \tag{1}$$

where c is the velocity of light in free space and ε_r is the dielectric constant of the antenna substrate.

Next, various stubs are attached to the main radiator to design bent monopoles with different resonating frequencies. Except for the smallest stub designed for mm-wave bands, all other stubs consist of horizontal and vertical parts. The overall length of each stub is optimized carefully for extra resonances at 2.5, 3.5, 5.5, and 7.5 GHz, and 5G mm-wave bands. For easy understanding, the step-by-step design procedure of the proposed antenna and their corresponding s-parameters $|S_{11}|$ are depicted in Figs. 3 and 4, respectively. It is noted that all these antennas have the same lateral size.

First, a stub of width w is loaded to the extreme left of the main radiator to get the resonance at a lower frequency.

This antenna (antenna-1) has two resonances: 1) the primary resonance due to the source antenna at 8.5 GHz and 2) the extra resonance at 2.5 GHz. The overall length of the monopole resonating at 2.5 GHz ($L_{2.5\text{GHz}}$) equals

$$L_{2.5\text{GHz}} = l_1 + w_1 + w_o = \frac{\lambda_{2.5\text{GHz}}}{4}. \tag{2}$$

Here, $\lambda_{2.5\text{GHz}}$ is the wavelength at 2.5 GHz.

Similarly, more stubs, working as folded monopoles, are added next to the first one with a spacing of $s = 1$ mm to achieve resonances at 3.5, 5.5, and 7.5 GHz. For convenience, the antenna with two, three, and four stubs are denoted as antenna-2, antenna-3, and antenna-4, respectively. The overall lengths of these resonating stubs can be computed as

$$L_{3.5\text{GHz}} = l_2 + w_2 = \frac{\lambda_{3.5\text{GHz}}}{4} \tag{3}$$

$$L_{5.5\text{GHz}} = l_3 + w_3 = \frac{\lambda_{5.5\text{GHz}}}{4} \tag{4}$$

$$L_{7.5\text{GHz}} = l_4 + w_4 = \frac{\lambda_{7.5\text{GHz}}}{4}. \tag{5}$$

Traditionally, the resonating monopole antennas are featured as narrow bandwidth [35], particularly at the lower frequencies, at 2.5 (7.2%) and 3.5 GHz (9.5%), as seen in Fig. 4. The limited bandwidth at these important bands, providing long-range connectivity to the IoT, can raise questions on the usage of the antenna. To overcome this problem, two additional stubs are attached at the backside of the antenna through the shorting pins (antenna-6 and antenna-7). These stubs are tuned carefully to give resonance at the neighboring frequencies (2.4 and 3.7 GHz) of 2.5 and 3.5 GHz to overlap these individual resonances for bandwidth improvement. It improved bandwidth to 11% at the 2.5-GHz band and 17% at the 3.5-GHz band.

Next, to provide a coverage for the 5G IoT at the mm-wave band (24/26/28 GHz), a horizontal stub of length (l_5) is added at the right corner of the basic rectangular monopole, represented as antenna-5. The length of the mm-wave stub ($L_{26\text{GHz}}$) is equal to

$$L_{28\text{GHz}} = l_5 = \frac{\lambda_{28\text{GHz}}}{4}. \tag{6}$$

Note that the antenna gives a resonance from 22 to 33.9 GHz at the mm-wave band. In summary, the proposed single-element antenna design gives resonances at 2.5, 3.5, 5.5, 7.5, and 24/26/28 GHz; this fully coves the microwave and mm-wave bands to provide uninterrupted connectivity for 5G IoT.

For the further demonstration of the radiation mechanism of the proposed antenna, the surface current distribution on antenna at various resonant frequencies is shown in Fig. 5. As expected, the current is mainly concentrated in the first (largest stub at the extreme left-hand side) monopole at 2.4 GHz. While at 3.5 GHz, the current is prominent at the second resonant monopole, reflecting the origin of the resonance. Similarly, at 5.5, 7.5, and 28 GHz, respectively, the third, fourth, and fifth monopoles resonate (i.e., they exhibit the highest current concentrations).

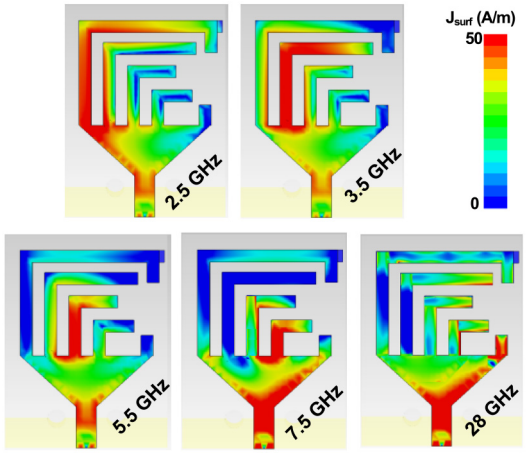

Fig. 5. Current distribution of the antenna at various resonant frequencies.

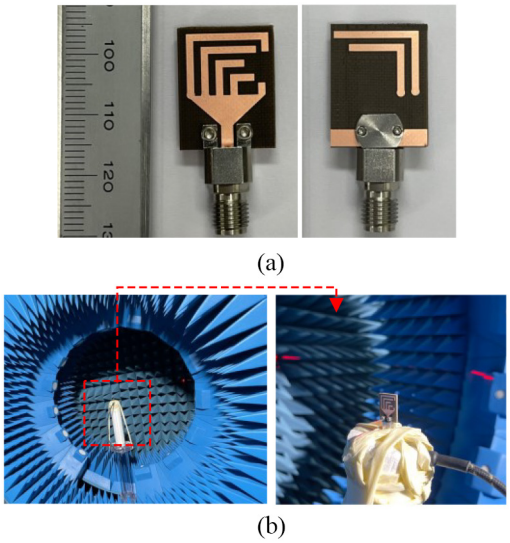

Fig. 6. Proposed integrated microwave and mm-wave antenna's (a) fabricated prototype and (b) measurement setup.

C. Results and Discussion

The single-element antenna is fabricated through photolithography with high-precision level to validate the simulated results. The antenna is fed with a 2.92-mm wave end-launch connector. The snapshots of the fabricated prototype and the measurement setup are shown in Fig. 6. The antenna is measured in a far-field measurement (multiprobe anechoic chamber) facility at Electromagnetic Wave Technology Institute, Seoul, South Korea. The s-parameter is measured in open air condition in a network analyzer (E8364B) by Agilent Technologies. Overall, the measurement results show good agreement with the simulated results.

$|S_{11}|$ of the proposed single-element antenna at microwave and mm-wave band is plotted in Fig. 7. The measurement results show that the antenna offers good impedance matching ($|S_{11}| < -10$ dB) from 2.37–2.65 GHz (11.15%), 3.25–3.85 GHz (16.9%), 5.0–6.1 GHz (19.8%), and 7.15–8.5 GHz (17.2%) at microwave frequency bands, while it resonates from 23–31 GHz (29.6%) at the mm-wave bands. This shows

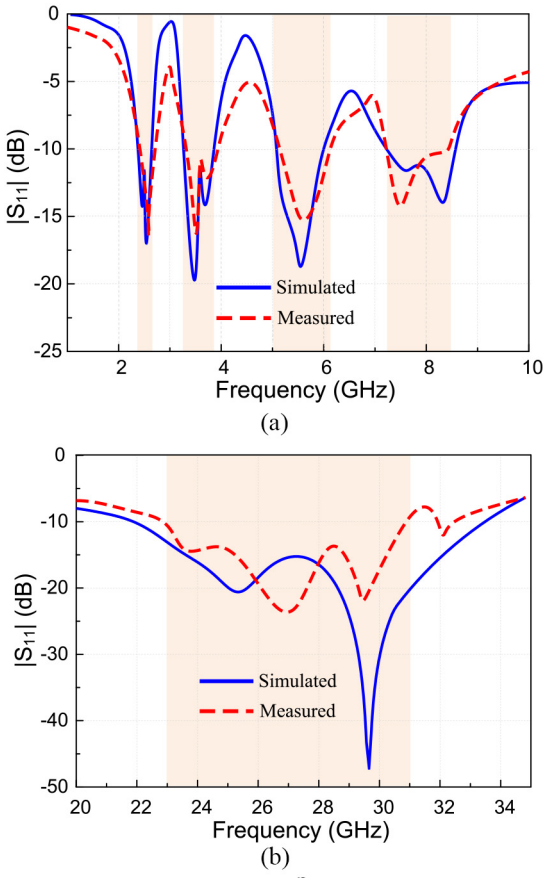

Fig. 7. Simulated and measured $|S_{11}|$ of the proposed antenna at: (a) microwave and (b) mm-wave bands.

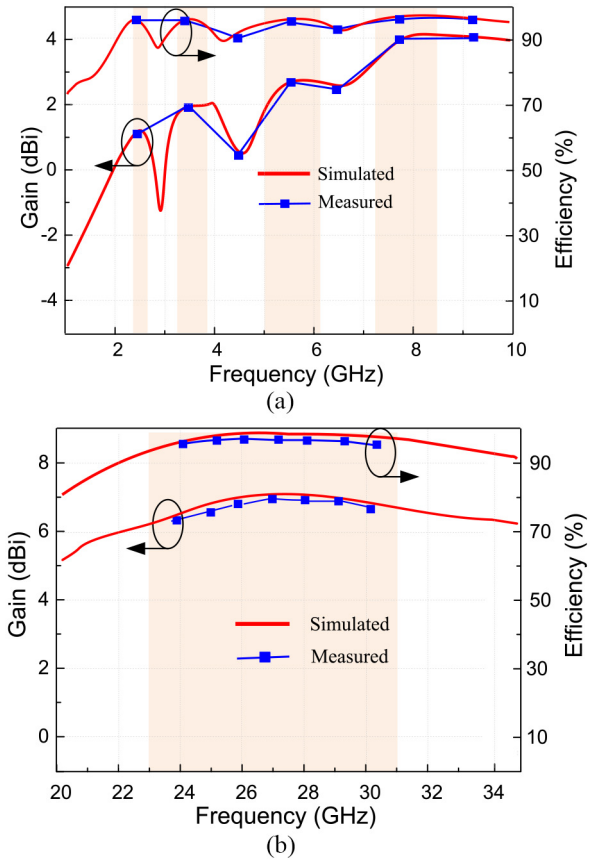

Fig. 8. Simulated and measured gain and radiation efficiency of the proposed antenna: (a) microwave and (b) mm-wave band.

that the antenna covers the important operating frequency bands, such as microwave bands for ISM-band (2.4 GHz), WLAN-band (2.5 and 5.5 GHz), 4G LTE band (2.5 GHz), 5G sub-6-GHz bands (2.5 and 3.5 GHz), and satellite downlink bands (7.5 GHz). Moreover, the antenna also covers designated mm-Wave bands (24–31 GHz) for 5G communications systems.

The gain and radiation efficiency characteristics of the antenna at microwave and mm-wave is plotted in Fig. 8. The antenna offers a gain level of more than 1 dBi at 2.5-GHz band, which increased to 2, 2.5, and 4 dBi at 3.5 GHz, 5.5 dBi, and 7.5 GHz, respectively. The gain increment with the increasing frequency is due to the increased effective antenna size at higher frequencies. At the same time, the gain is more than 6 dBi in the entire mm-wave bands. Moreover, the radiation efficiency is noted to be more than 95% at microwave and mm-wave bands due to the usage of the low-loss high-frequency substrate.

Fig. 9 shows the radiation pattern of the single-element antenna at 2.5, 3.5, 5.5, and 7.5 GHz. The antenna shows a radiation pattern of a conventional monopole antenna giving omnidirectional pattern at *xoz*-plane (phi = 0°) and dumbbell-shaped radiation patterns at *yoz*-plane (phi = 90°). Importantly, the radiation pattern is stable for all frequency bands due to the effective utilization of the individual resonances of the stubs.

The radiation pattern of the antenna at mm-wave bands is shown in Fig. 10. It is interesting to note that the antenna has a stable end-fire radiation pattern at the mm-wave band, where the main direction of maximum radiation is parallel with the antenna structure. The end-fire nature of the antenna is due to its quasi-yagi antenna geometry. The perpendicular microwave stubs in front of the mm-wave monopole are acting as directors to give high-gain end-fire radiations [36].

III. MIMO Antenna for 5G IoT Applications

The proposed single-element antenna is incorporated into various MIMO (2 × 2, 2 × 4, and 3 × 4 configurations) assemblies to exploit multipath propagation for the high-date rates, capacity, and link reliability through spatial and pattern diversity for its applications in future IoT communications.

A. 2 × 2 MIMO Antenna

First, the antenna is incorporated in 2 × 2 MIMO configuration by translating a single-element antenna orthogonally having a distance of d = 16 mm between the adjacent antennas. For the sake of isolation improvement, the adjacent antenna elements are printed on the backside of the substrate, while the diagonally positioned antennas are in the same plane of the substrate. The geometrical configuration and the fabricated prototype of the antenna are shown in Fig. 11. The simulated and measured transmission

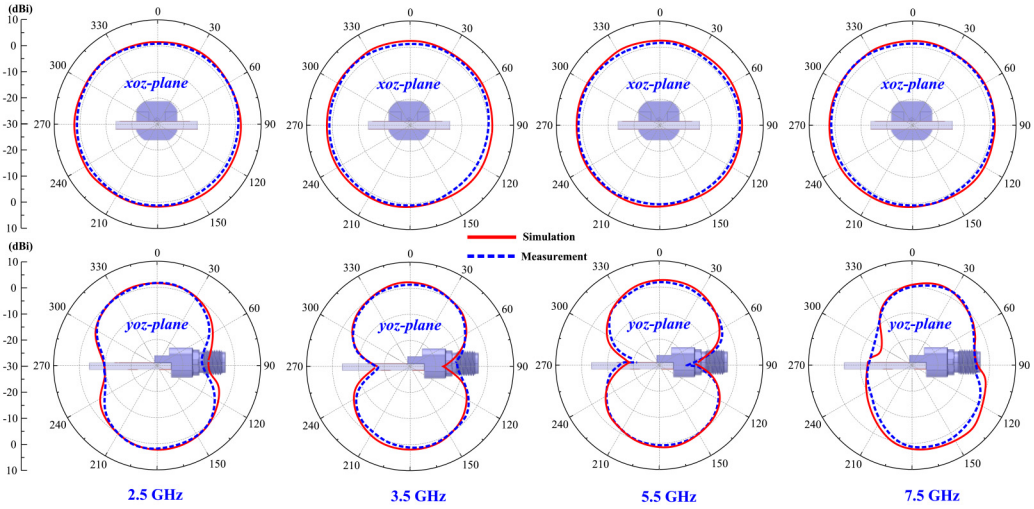

Fig. 9. Simulated and measured radiation patterns of the proposed antenna at microwave frequencies.

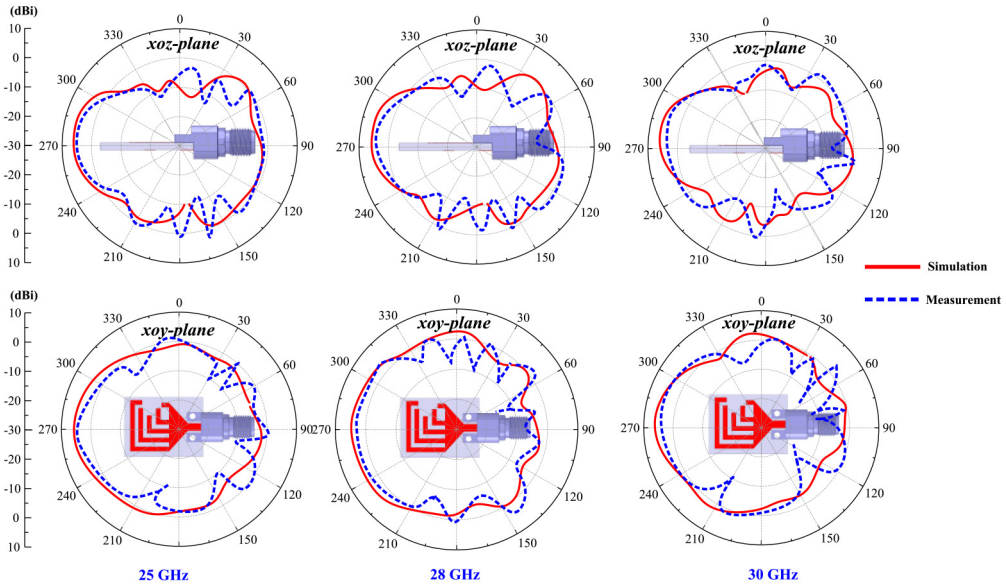

Fig. 10. Simulated and measured radiation patterns of the proposed antenna at mm-wave frequencies.

coefficients ($|S_{ij}|$) of the antenna revealed that the antennas offer high isolation of more than 20 dB (Fig. 12). Furthermore, the adjacent antennas offer the same simulated isolation characteristics ($|S_{21}|$, $|S_{32}|$, ($|S_{41}|$, $|S_{43}|$) due to the geometrical symmetry. Similarly, the orthogonally located antennas ($|S_{31}|$, $|S_{42}|$) have identical isolation among them. For brevity, only the measured value of $|S_{21}|$ and $|S_{31}|$ has been plotted. The average isolation between the diagonally located antennas is lower than the adjacent antennas as the distance among them is larger than the adjacent antennas. Here, the isolation for the mm-wave bands has not been shown, since it is very high because of the marked element spacing (16 mm $\approx 1.5\lambda$o at 27 GHz).

B. 2 × 4 MIMO Antenna

The 2 × 2 MIMO antenna is used for the design of the 2 × 4 MIMO system by flipping it 90° along its axis. This configuration adds the pattern diversity of the MIMO antennas in both azimuth and elevation planes. The antenna design parameters are the same as the 2 × 2 MIMO antenna. For practical realization, two prototypes of the 2 × 2 MIMO elements are used having a slot of 1.6 mm (equal to the thickness of the substrate) as shown in Fig. 13.

As the isolation is the key parameter in the MIMO system, its numerically computed and measured plots at the microwave band are exhibited in Fig. 14. The antennas offer good isolation due to their unique arrangement; every antenna is perpendicular to its adjacent antennas. The antennas facing each other (e.g., port-5 and port 1, port-6, and port-2) have relatively low isolation (<15 dB) at lower bands, while all other antennas have transmission coefficients of less than −20 dB. Again, only some representative isolation plots between the antenna ports have been shown for a clear illustration. The measured data follows the pattern of the simulated curve and has a good agreement with its counterpart.

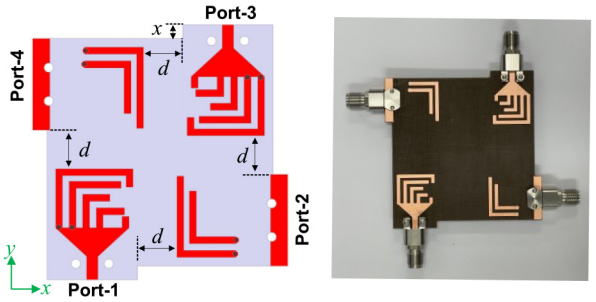

Fig. 11. Schematic and prototype of the 2 × 2 MIMO antenna ($d = 16$ mm and $x = 2$ mm).

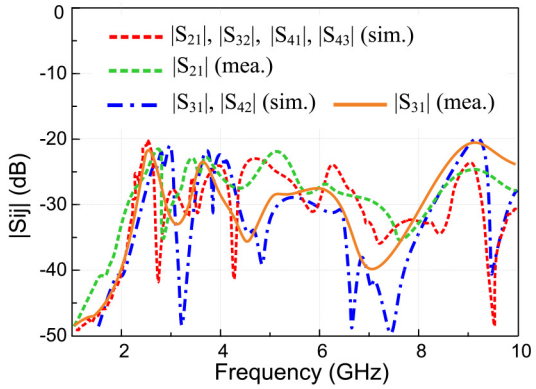

Fig. 12. Simulated and the measured reflection coefficients of the 2 × 2 MIMO antenna.

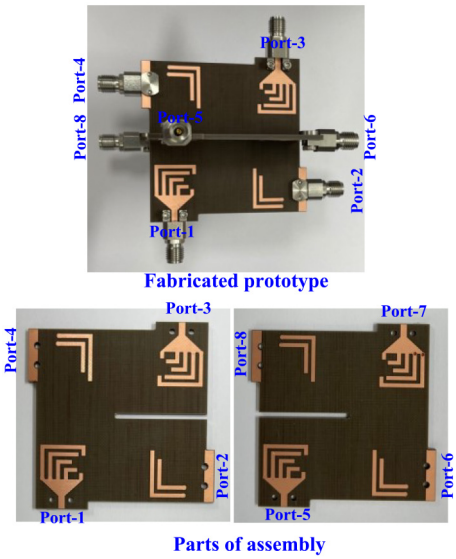

Fig. 13. Fabricated prototype of the 2 × 4 MIMO antenna.

C. 3 × 4 MIMO Antenna

MIMO systems with several antenna elements with pattern diversity and low mutual coupling are the fundamental requirement for the 5G IoT communications. Therefore a 3 × 4 MIMO antenna is designed using the 2 × 2 MIMO designed previously in Section III-A. This design is obtained by rotating the 2 × 2 MIMO antenna, one time on the x-axis and another time on y-axis. This allows the arrangement of

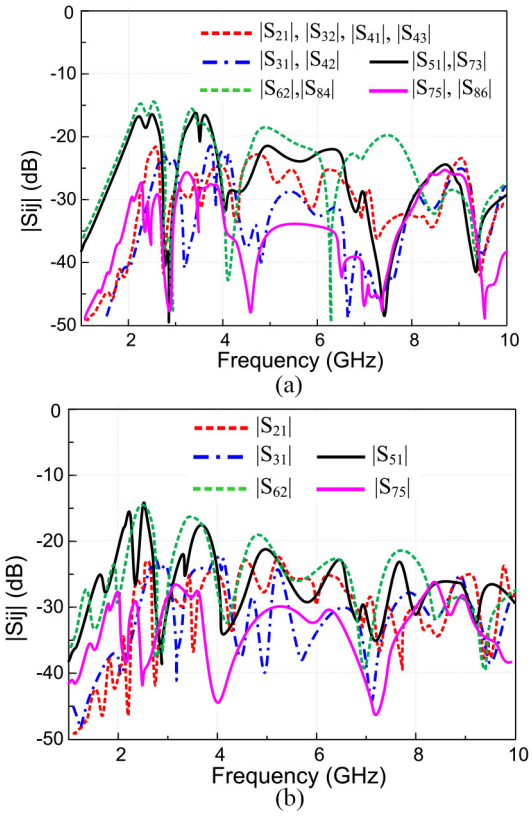

Fig. 14. Reflection coefficients of the 2 × 4 MIMO antenna: (a) simulated and (b) measured.

12 antenna elements in a three-dimensional (3-D) geometry to form the proposed 3 × 4 MIMO antenna system. The proposed 3 × 4 MIMO antenna's geometry and fabricated prototype with its parts of the assembly are shown in Fig. 15.

It can be seen from the parts of the assembly that the proposed MIMO system consists of three units of planar 2 × 2 MIMO antenna; two units have a vertical slot, and one has a "plus-shaped" slot. These three units are arranged in the formation of the unique 3-D MIMO system. Therefore, the particular antenna has the advantages of mass production suitability with low-cost fabrication.

The simulated and measured isolation among antenna elements in this MIMO system is plotted as transmission coefficient in Fig. 16. Like the 2 × 4 MIMO antenna, the isolation among the antenna ports is more than 20 dB for all antennas except for those antennas which are facing each other (for example, port-5 and port-1, port-5 and port-2, port-11 and port-3, port-11 and port 2, etc.). Moreover, the antennas facing each other have an orthogonal arrangement, this gives radiation diversity and thereby have low coupling between the antennas. The isolation values of these antennas are more than 15 dB across the designated microwave bands, which are good enough for uninterrupted communications in 5G IoT.

To explore the radiation stability and beam diversity, the radiation patterns at selected ports (port-1, port-5, and port-6) are measured at various frequencies (2.5, 3.5, 5.5, and

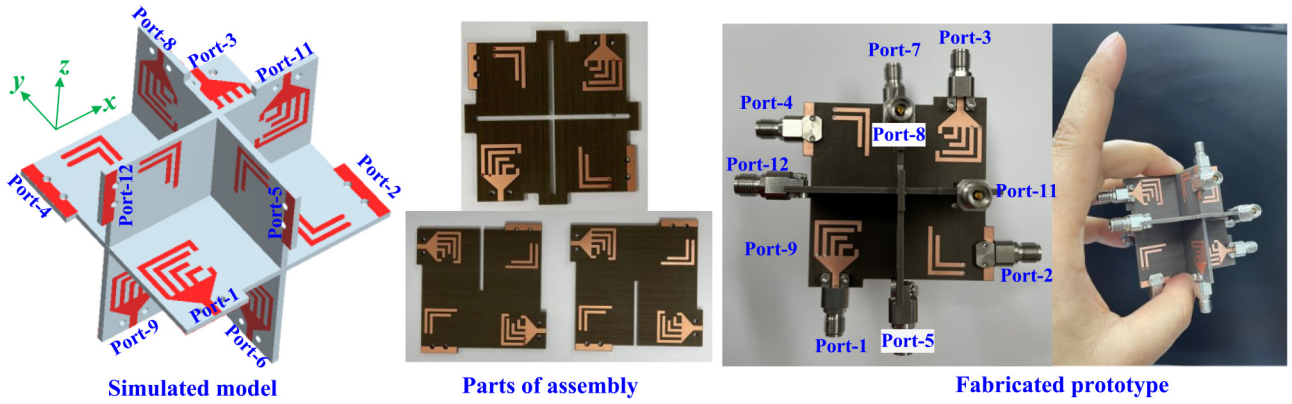

Fig. 15. Configuration and the fabricated prototype of the 3 × 4 MIMO antenna.

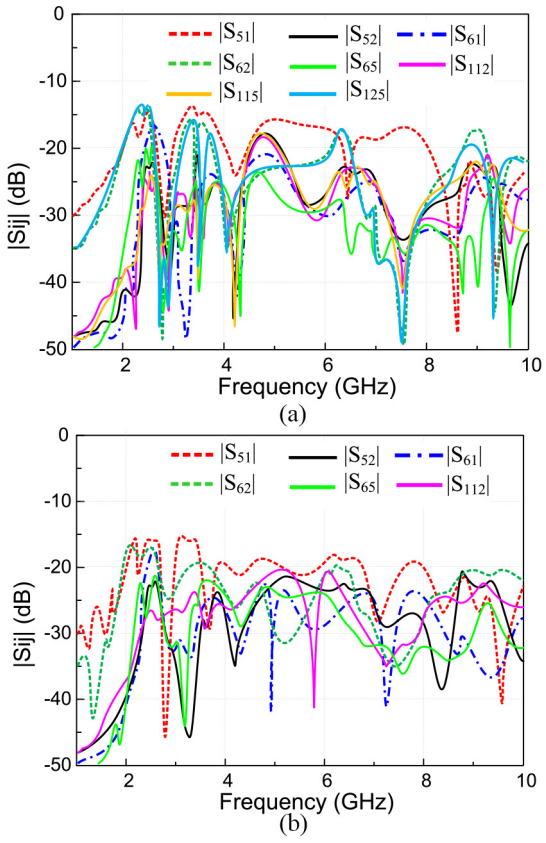

Fig. 16. S-parameters of the 3 × 4 MIMO antenna: (a) simulated and (b) measured.

7.5 GHz) and compared with the simulated pattern (Fig. 17). It is obvious from the antenna geometry (Fig. 15) that all the 12-antennas are identical, with the only difference being their direction of propagation. The antenna for port-1 shows a quasidirectional radiation pattern having a narrow half-power-beamwidth (HPBW); the main beam toward 180° at *xoz*-plane (phi = 0°). However, the radiations are mostly directed toward 120° at *yoz*-plane (phi = 90°) with a wider HPBW. Interestingly, the radiation patterns of the antenna for port-5 show a mirror transformation of 180° in both planes due to radiating orientation. That means, more radiations for port-1 are directed toward 0° and 300° in *xoz*-plane and *yoz*-plane, respectively. However, for port-6, the narrow beam is directed toward 90° in *xoz*-plane and the radiation pattern with wide HPBW is around 60° in *xoy*-plane. In the same fashion, the radiation patterns of other antennas can also be predicted. Due to identical monopoles, almost the same gain values are observed for all antennas at specific frequencies. It is worth noting that the radiation pattern of the antennas in the 3 × 4 MIMO system becomes quasidirectional at both planes, while it was omnidirectional at one plane and bidirectional (dumbbell shape) at another plane. This is because the neighboring facing antennas radiations are reflecting the main beam in the direction of open space. To understand this, let us consider the radiations of the antenna-1. This antenna is surrounded by antenna-5 and antenna-6 in the *x*-plane, while antenna-9 and antenna-12 in *y*-plane. Therefore, the antenna's main beam is prominent in the direction of the vacant space. Thereby, the omnidirectional radiations (in case of single-element) are tilted toward 180° at *xoz*-plane, while the bidirectional beams are focused at 120° at *yoz*-plane.

The multipath losses can be avoided if the antenna elements in the MIMO system offer pattern diversity, that is, propagation of radiation in different planes (directions). The pattern diversity also improves the quality and reliability of a wireless link of the IoT devices by providing coverage in all directions.

To demonstrate the pattern diversity of the proposed 3 × 4 MIMO module, the radiation patterns for some antenna elements (port-1 to port-4) at 3.5 GHz for *xoy*- and *xoz*-planes have been plotted in Fig. 18. It is evident from the figure that each antenna is radiating toward a specific direction. In both planes, the beams are directed toward 180°, 90°, 0°, and 270° for port-1, port-2, port-3, and port-4, respectively. In the same manner, the rest of the antennas also provide pattern diversity at various directions to offer 360-degrees coverage in azimuth and elevation planes. The separate ground planes and the orthogonal arrangement of antenna elements in this provide suppression of near-field coupling for the adjacent antenna elements for high port-to-port isolation and uncorrelated radiation patterns.

The radiation patterns of the mm-wave antennas (port-1 to 4) at 25 and 28 GHz have been shown in Fig. 19. Since

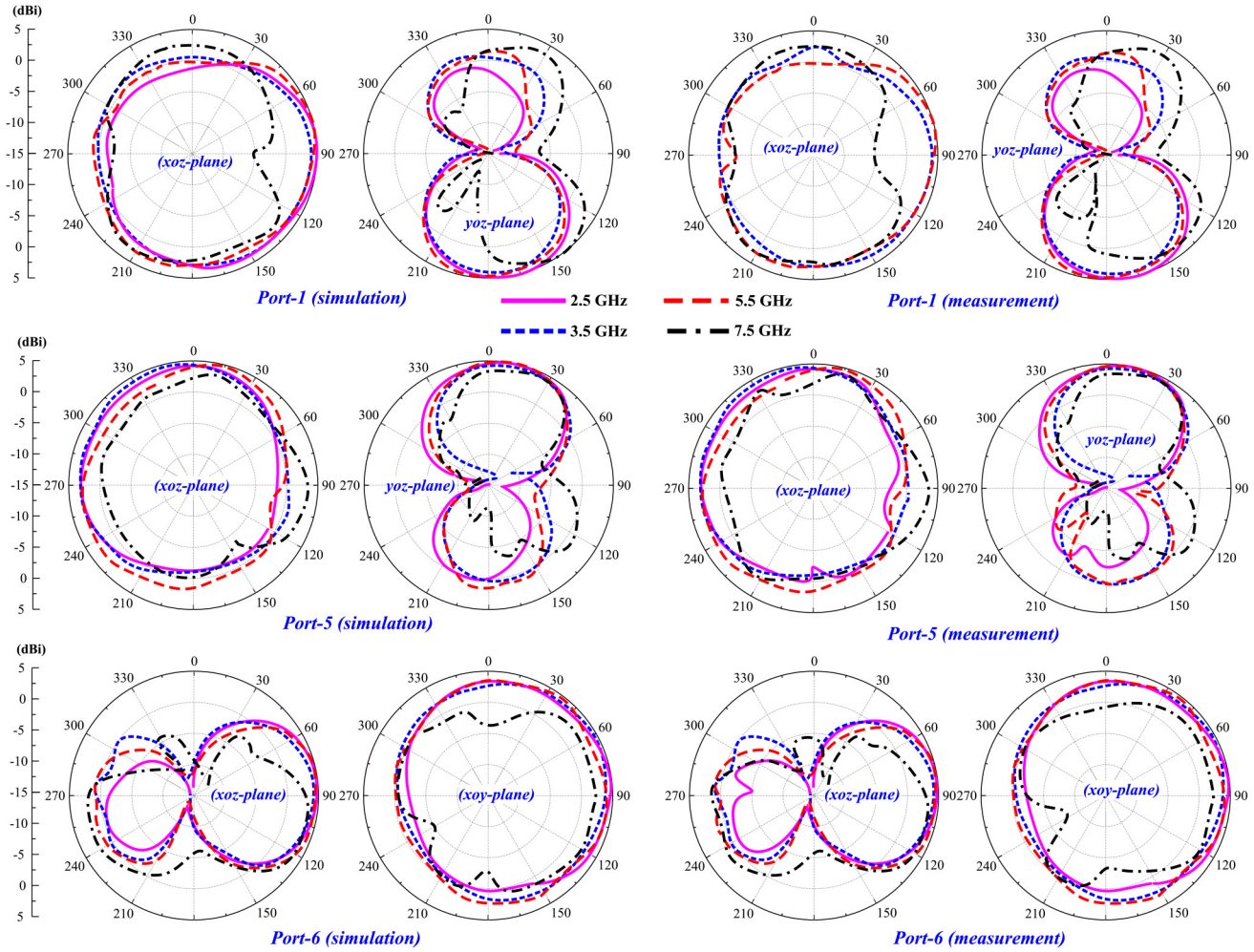

Fig. 17. Radiation patterns of the proposed 3 × 4 MIMO antenna at microwave bands.

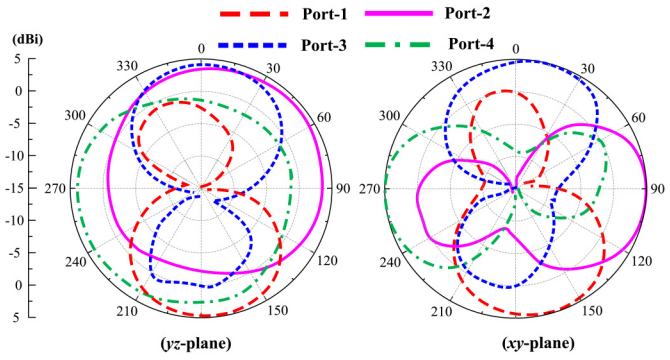

Fig. 18. Demonstration of uncorrelated radiation patterns of the 3 × 4 MIMO antenna at 3.5 GHz; the pattern diversity coverage is 360°.

the mm-wave antennas have end-fire radiation patterns, each antenna radiates in different directions. For example, antenna-1 (port-1) has the main beam toward 270° in *xoz*- and *yoz*-planes. Similarly, the antenna for Port-2 radiates toward 0°. While antennas for Port-3 and 4 have more radiations in the direction of 90° and 180°, respectively. Again, the mm-wave antennas also offer radiation pattern diversity. Noting that the antennas for other ports (Port-5 to 12) have also specific directions for coverage based on their orientation.

IV. Application Scenarios

Since the proposed antenna covers the important IoT bands of microwave and mm-wave bands, the antenna can be used in various applications ranging from indoor communications in smart houses, offices, shopping malls, bus stops, and vehicle-to-everything (V2X) communications. Few application scenarios are explained below in detail.

A. Indoor Communication Systems

The indoor communication in future smart houses and shopping malls will be using microwave and mm-wave bands to support multisystem communication, as portrayed in Fig. 20. The microwave bands will provide long-range communications with medium speed to connect a huge number of IoT devices and multimedia gadgets, while the mm-wave bands will offer short-range high-data rates with ultralow latency communications for ultrahigh-definition multimedia, augmented reality, games, data devices, and more. Our antenna smoothly transmits and receives high-frequency signals in any direction of 360°. There is no reception shadow area and broadband high-capacity reception is possible due to the realization of a high-isolation 12-port MIMO antenna with pattern diversity at both microwave and mm-wave bands.

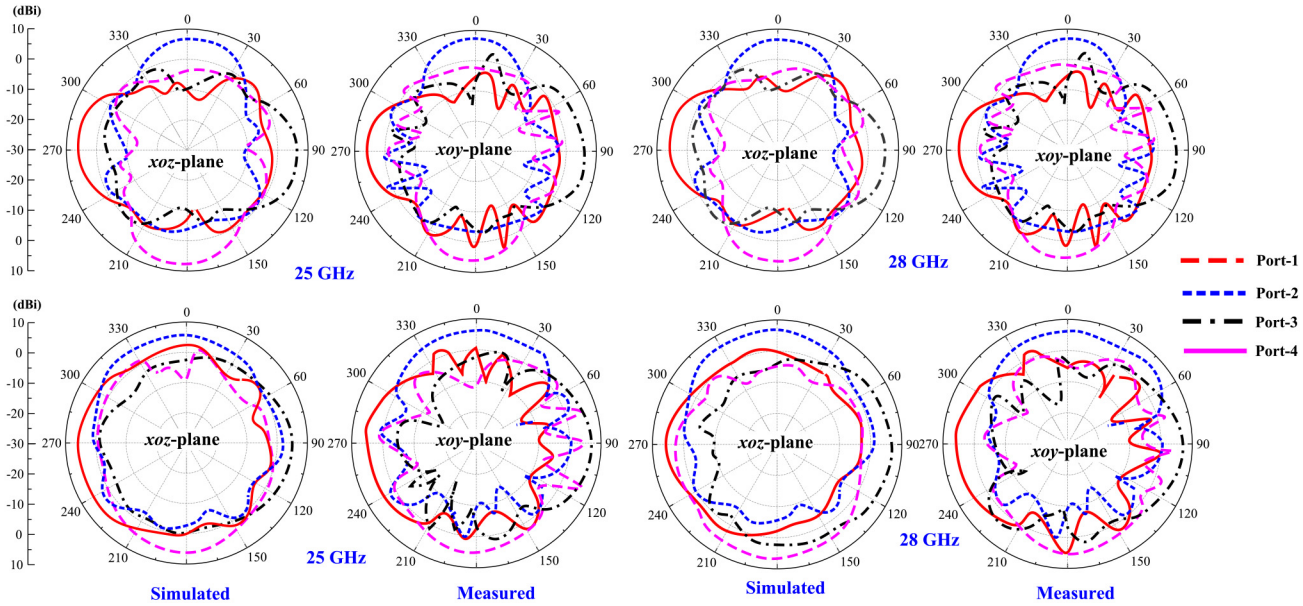

Fig. 19. Radiation patterns of the proposed 3 × 4 MIMO antenna at mm-wave bands.

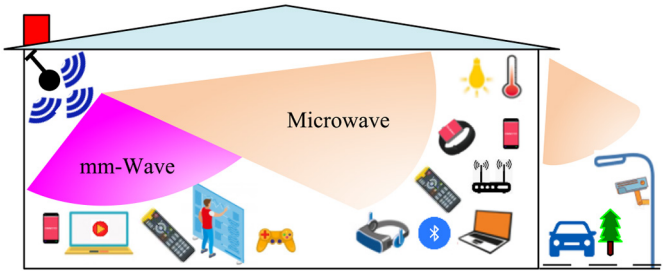

Fig. 20. Indoor application of the proposed microwave and mm-wave MIMO antenna; long-range medium-speed and short-range ultrafast communications are possible.

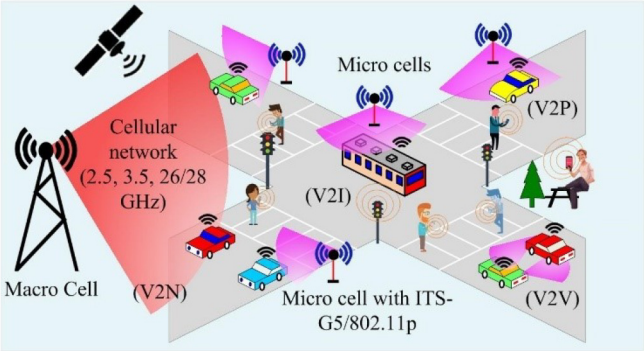

Fig. 21. Application of the proposed microwave and mm-wave MIMO antenna in V2X communications.

B. V2X Communication Systems

Fig. 21 shows that the antenna can be installed in cars of an ITS allowing vehicle-to-vehicle communication in the ITS-G5/802.11p band (5.9 GHz). The vehicles can communicate with infrastructure (V2I) using the ISM bands (2.4 and 5.8 GHz), WLAN bands (2.5 and 5.5 GHz), Bluetooth band (2.4 GHz), and satellite downlink band (7.5 GHz) [37], [38]. Moreover, using the 5G cellular bands (2.5, 3.5, and 24/26/28 GHz), the vehicles can communicate with a cellular network (V2N) and pedestrians (V2P). Because of the uncorrelated radiation pattern diversity and high-level isolation of the antenna elements, our antenna facilitates full-duplex operation, thus connecting everything in a V2X scenario.

The 12-port MIMO antenna module is simulated with a full car model to see the antenna behavior. The antenna is placed at a distance of 10 mm above the car body to isolate it from the conducting car body [39]. This can be realized in a practical scenario using a nonconducting aerodynamic antenna housing. The simulation setup and radiation pattern of the antenna for port 1 to 4 at 5.8 GHz at various ports are shown in Fig. 22. The antennas retain their radiation characteristics with a beam diversity, even when installed on the car body. In addition, the multiple antennas in the MIMO system are responsible to process transmission and reception simultaneously to provide full coverage for an uninterrupted link in V2X communications.

A link budget analyzes the performance of the communication channel considering all the losses that a communication link observes in a communication system. The MIMO antenna module's link budget is calculated at 5.9 GHz (ITS-G5/802.11p band) to determine its suitability for V2X communication, utilizing the following relation [40]:

$$P_{\text{rec}} = P_{\text{tran}} + T_G - L_T - L_P + L_M + R_G - L_R \tag{7}$$

where P_{rec} is the received power in dBm and P_{tran} is the transmission power in dBm; T_G is the gain of the transmitter antenna; L_T is the loss at the transmitting end; L_P is the overall free space path loss between the transmitting and receiving antennas; L_M is miscellaneous losses, including the fade margin and polarization misalignment; R_G is the receiver antenna gain; and L_R is the total loss at the receiving end.

TABLE I
PERFORMANCE COMPARISON WITH STATE-OF-THE-ART INTEGRATED MICROWAVE AND MM-WAVE ANTENNAS

Antennas	Antenna type	Operating Microwave bands (GHz)	Operating mm-wave bands (GHz)	Single port for all bands?	Beam coverage of the MIMO antennas	
					Microwave band	mm-wave band
[24]	Dipole+ tapered slot	3.6	28	No	Fixed beam	120° in θ-direction
[25]	PIFA+leaky wave	2.4, 5.2	60	No	Fixed beam	72° in θ-direction
[26]	Patch + Dipole	2.4, 5	60	No	Fixed beam	Fixed beam
[27]	Fabry-Perot Resonator	2.4	24	No	Fixed beam	Fixed beam
[28]	Patch + SIW slot	7	38	No	72° θ-direction	81° in θ-direction
[29]	Patch + Dipole	3.5	28	No	Fixed beam	68° in θ-direction
[31]	Slotted monopole	2.5, 5.5	26	No	Fixed beam	360°in θ-direction
[32]	SIW Slot array	3, 6	28, 38	No	Fixed beam	Fixed beam
[33]	Slot based monopole	Six sub-6 GHz bands	28	No	Fixed beam	Fixed beam
[34]	Slotted monopole	3.5	28, 38	Yes	Fixed beam	Fixed beam
Proposed antenna	Monopole + stubs	2.5/3.5/5.5/7.5	28	Yes	360° in θ-direction 360° in φ -direction	360°in θ-direction 360°in φ -direction

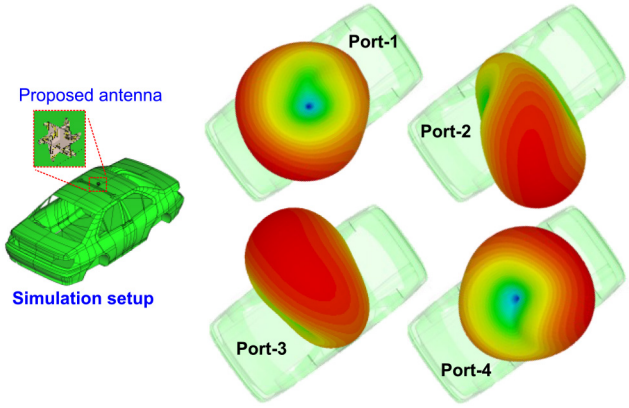

Fig. 22. Simulation setup and radiation patterns of the proposed MIMO antenna on the roof of the car model for different port excitation at 5.9 GHz.

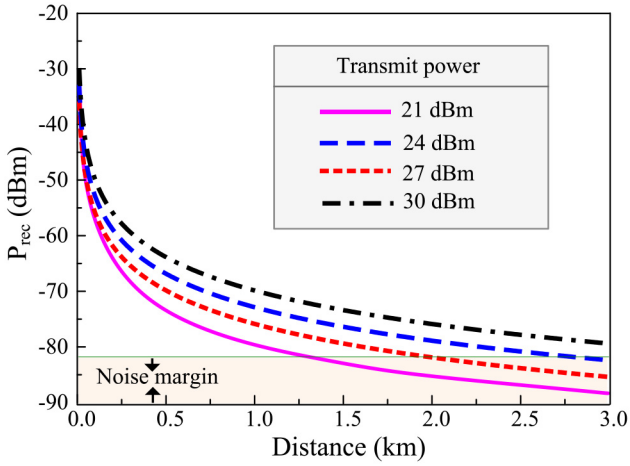

Fig. 23. Link budget of the proposed MIMO antenna at 5.9 GHz for various transmit powers.

All other parameters for a given communication system are fixed [$T_G = R_G = 3$ dBi, $L_T \approx 3.2$ dB, $L_M \approx 0.5$ dB, and $L_R \approx 2.35$ dB], except L_P, which varies for distance and frequency. The path loss L_P can be estimated as [41]

$$L_{P(\mathrm{dB/km})} = 32.4 + 20\log_{10}(d_{\mathrm{km}}) + 20\mathrm{Log}_{10}(f_{\mathrm{MHz}}). \quad (8)$$

The minimum signal power (sensitivity) that the proposed antenna can detect is calculated using the method given in [42], which is found to be -82 dBm.

However, the Federal Communication Commission and World Health Organization are recommending antenna power up to 30 dBm for urban areas. The 5G automotive association (5GAA) is restricting transmit power to 21 dBm for the V2X communication [43]. The link budget of the proposed integrated microwave and mm-wave antenna at 5.9 GHz for various transmit powers is shown in Fig. 23. It shows that the antenna can offer a stable link for V2X communication over a wide distance of > 1.25 km for a transmit power of 21 dBm; this greatly exceeds the 5GAA standard of 0.3 km.

V. PERFORMANCE COMPARISON

The proposed integrated microwave and mm-wave antenna module is compared with the related state-of-the-art works in Table I. Most of the integrated antennas [26], [27], [32]–[34] have few operating frequency bands with one direction of propagation. That is, the coverage area is limited to a fixed direction. The antennas proposed in [24], [25], [29], [31] offer a wide coverage area in mm-wave bands; however, the microwave band patterns have fixed beams toward a single direction. Although the antenna design [28] has flexible beam coverage, it is limited to a maximum of 80° space coverage in the θ-direction. The multiband antenna [33] offers the advantages of the various operating microwave frequency bands (six

sub-6-GHz bands) have the limitations of the single direction of propagation. Only our antenna has the capability of 360° full space coverage in both theta and phi-directions with the additional advantages of wideband resonances at the essential microwave bands (2.5, 3.5, 5.5, and 7.5 GHz) and mm-wave bands (23–31 GHz). It is worth noting that none of the antennas in the literature support both microwave and mm-wave bands with a single feeding port, except [34]. Nevertheless, it has only three operating bands (3.5, 28, and 38 GHz), and all antennas have the same propagation direction. In other words, our 12-port MIMO system is the only one of its kind that offers the codesign of microwave and mm-wave antenna with a single input port. Besides, it is capable of complete 360° space coverage in elevation and azimuth planes for full-duplex operations to provide seamless connectivity in modern devices and sensors.

VI. Conclusion

The integration of microwave and mm-wave band antennas in a single design for the multistandard IoT system is a challenging task due to the large frequency ratio. We developed a multiband 12-port MIMO antenna operating at microwave bands (2.5/3.5/5.5/7.5-GHz bands) and mm-wave bands, offering high isolation and pattern diversity for 5G IoT applications. The single-element antenna features a printed triangular monopole with resonating stubs (five on the front and two on the back). The two stubs in the back are connected to the central radiator (with metallic pins) for the bandwidth improvements at 2.5- and 3.5-GHz bands. The multiband characteristics are obtained by adding five inverted L-shaped resonating stubs to a monopole on its front side. Two stubs are inserted at the backside of the antenna, through metallic pins for bandwidth improvements at 2.4- and 3.5-GHz bands. Simulation and measured results show that the antenna operates at key important bands of 2.5-GHz band (2.37–2.65 GHz), 3.5-GHz band (3.25–3.85 GHz), 5.5-GHz band (5.0–6.1 GHz), and 7.5-GHz band (7.15–8.5 GHz). Besides, it also gives resonance at 5G mm-wave bands (23–31 GHz) with suitable radiation characteristics.

The single-element antenna is translated to design 2×2 MIMO antenna, which is further used in the designing of 2×4 and the proposed 3×4 MIMO system to provide spectral and pattern diversity. The proposed 12-port MIMO module has the advantages of good isolation (less than 15 dB at the lowest frequency band of 2.5-GHz band) and pattern diversity for 360° space coverage for full-duplex operations to provide seamless connectivity for modern devices and sensors. Furthermore, the antenna's application scenarios in indoor and V2X communication are discussed. The link budget is also calculated to find the antenna's suitability for V2X communications, which shows that the antenna can communicate within the acceptable noise margin over a distance of 1.25 km with a 21 dBm of transmit power. Owing to these qualities, the proposed MIMO antenna can be an excellent choice for V2X MIMO communications. To our knowledge, the proposed antenna is the first of its kind that has the ability to cover all the key frequency bands from microwave to mm-wave bands with polarization diversity and high isolation, making it a good candidate for 5G IoT applications.

Since the antenna elements has fixed radiation patterns that may trigger intercell interferences, future research will focus on beam steering and enhanced gain characteristics.

References

[1] L. Chettri and R. Bera, "A comprehensive survey on Internet of Things (IoT) toward 5G wireless systems," *IEEE Internet Things J.*, vol. 7, no. 1, pp. 16–32, Jan. 2020.

[2] A. Zanella, N. Bui, A. Castellani, L. Vangelista, and M. Zorzi, "Internet of Things for smart cities," *IEEE Internet Things J.*, vol. 1, no. 1, pp. 22–32, Feb. 2014.

[3] A. Gupta and R. K. Jha, "A survey of 5G network: Architecture and emerging technologies," *IEEE Access*, vol. 3, pp. 1206–1232, 2015.

[4] "Cisco annual Internet report (2018-2023)," Cisco, San Jose, CA, USA, White Paper. Accessed: Jan. 2022. [Online]. Available: https://www.cisco.com/c/en/us/solutions/collateral/executive-perspectives/annual-internet-report/white-paper-c11-741490.html

[5] Y. Wang, J. Zhang, F. Peng, and S. Wu, "A glasses frame antenna for the applications in Internet of Things," *IEEE Internet Things J.*, vol. 6, no. 5, pp. 8911–8918, Oct. 2019.

[6] R. Rodriguez-Cano and R. W. Ziolkowski, "Single-layer, unidirectional, broadside-radiating planar quadrupole antenna for 5G IoT applications," *IEEE Trans. Antennas Propag.*, vol. 69, no. 9, pp. 5224–5233, Sep. 2021.

[7] B. Xiao, H. Wong, D. Wu, and K. L. Yeung, "Design of small multiband full-screen smartwatch antenna for IoT applications," *IEEE Internet Things J.*, vol. 8, no. 24, pp. 17724–17733, Dec. 2021.

[8] T. Leng, K. Pan, X. Zhou, Y. Li, M. A. Abdalla, and Z. Hu, "Non-volatile RF reconfigurable antenna on flexible substrate for wireless IoT applications," *IEEE Access*, vol. 9, pp. 119395–119401, 2021.

[9] K. R. Jha, B. Bukhari, C. Singh, G. Mishra, and S. K. Sharma, "Compact planar multistandard MIMO antenna for IoT applications," *IEEE Trans. Antennas Propag.*, vol. 66, no. 7, pp. 3327–3336, Jul. 2018.

[10] T. Houret, L. Lizzi, F. Ferrero, C. Danchesi, and S. Boudaud, "DTC-enabled frequency-tunable inverted-F antenna for IoT applications," *IEEE Antennas Wireless Propag. Lett.*, vol. 19, no. 2, pp. 307–311, Feb. 2020.

[11] C. T. Liao, Z. K. Yang, and H. M. Chen, "Multiple integrated antennas for wearable fifth-generation communication and Internet of Things applications," *IEEE Access*, vol. 9, pp. 120328–120346, 2021.

[12] N. Hussain, A. Abbas, S. M. Park, S. G. Park, and N. Kim, "A compact tri-band antenna based on inverted-L stubs for smart devices," *Comput. Mater. Continua*, vol. 70, no. 2, pp. 3321–3331, 2022.

[13] H. T. Chattha, M. K. Ishfaq, B. A. Khawaja, A. Sharif, and N. Sheriff, "Compact multiport MIMO antenna system for 5G IoT and cellular handheld applications," *IEEE Antennas Wireless Propag. Lett.*, vol. 20, no. 11, pp. 2136–2140, Nov. 2021.

[14] Y. Yao, X. Cheng, C. Wang, J. Yu, and X. Chen, "Wideband circularly polarized antipodal curvedly tapered slot antenna array for 5G applications," *IEEE J. Sel. Areas Commun.*, vol. 35, no. 7, pp. 1539–1549, Jul. 2017.

[15] Z. Cai, Y. Zhou, Y. Qi, W. Zhuang, and L. Deng, "A millimeter wave dual-lens antenna for IoT-based smart parking radar system," *IEEE Internet Things J.*, vol. 8, no. 1, pp. 418–427, Jan. 2021.

[16] N. Hussain, M. Jeong, A. Abbas, and N. Kim, "Metasurface-based single-layer wideband circularly polarized MIMO antenna for 5G millimeter-wave systems," *IEEE Access*, vol. 8, pp. 130293–130304, 2020.

[17] M. Wagih, G. S. Hilton, A. S. Weddell, and S. Beeby, "Millimeter wave power transmission for compact and large-area wearable IoT devices based on a higher-order mode wearable antenna," *IEEE Internet Things J.*, vol. 9, no. 7, pp. 5229–5239, Apr. 2022.

[18] N. Hussain, M. Jeong, A. Abbas, T. Kim, and N. Kim, "A metasurface-based low-profile wideband circularly polarized patch antenna For 5G millimeter-wave systems," *IEEE Access*, 8, pp. 22127–22135, 2020.

[19] P. Burasa, T. Djerafi, and K. Wu, "A 28 GHz and 60 GHz dual-band on-chip antenna for 5G-compatible IoT-served sensors in standard CMOS process," *IEEE Trans. Antennas Propag.*, vol. 69, no. 5, pp. 2940–2945, May 2021.

[20] A. K. Arya, S. Kim, K. Ko, and S. Kim, "Antenna for IoT-based future advanced (5G) railway communication with end-fire radiation," *IEEE Internet Things J.*, vol. 9, no. 9, pp. 7036–7042, May 2022.

[21] E. M. Wissem, I. Sfar, L. Osman, and J.-M. Ribero, "A textile EBG-based antenna for future 5G-IoT millimeter-wave applications," *Electronics*, vol. 10, no. 2, p. 154, 2021.
[22] R. Hussain, "Dual-band-independent tunable multiple-input–multiple-output antenna for 4G/5G new radio access network applications," *IET Microw. Antennas Propag.*, vol. 15, no. 3, pp. 300–308, 2021.
[23] M. Ikram, N. Nguyen-Trong, and A. M. Abbosh, "Realization of a tapered slot array as both decoupling and radiating structure for 4G/5G wireless devices," *IEEE Access*, vol. 7, pp. 159112–159118, 2019.
[24] M. Ikram, N. Nguyen-Trong, and A. M. Abbosh, "Common-aperture sub-6 GHz and millimeter-wave 5G antenna system," *IEEE Access*, vol. 8, pp. 199415–199423, 2020.
[25] Y. R. Ding and Y. J. Cheng, "A tri-band shared-aperture antenna for (2.4, 5.2) GHz Wi-Fi application with MIMO function and 60 GHz Wi-Gig application with beam-scanning function," *IEEE Trans. Antennas Propag.*, vol. 68, no. 3, pp. 1973–1981, Mar. 2020.
[26] X. Yang *et al.*, "An integrated tri-band antenna system with large frequency ratio for WLAN and WiGig applications," *IEEE Trans. Ind. Electron.*, vol. 68, no. 5, pp. 4529–4540, May 2021.
[27] L. Y. Feng and K. W. Leung, "Dual-frequency folded-parallel-plate antenna with large frequency ratio," *IEEE Trans. Antennas Propag.*, vol. 64, no. 1, pp. 340–345, Jan. 2016.
[28] Y. Li and J. Wang, "Dual-band leaky-wave antenna based on dual- mode composite microstrip line for microwave and millimeter-wave applications," *IEEE Trans. Antennas Propag.*, vol. 66, no. 4, pp. 1660–1668, Apr. 2018.
[29] J. Lan, Z. Yu, J. Zhou, and W. Hong, "An aperture-sharing array for (3.5, 28) GHz terminals with steerable beam in millimeter-wave band," *IEEE Trans. Antennas Propag.*, vol. 68, no. 5, pp. 4114–4119, May 2020.
[30] Y. Sun and K. W. Leung, "Substrate-integrated two-port dual-frequency antenna," *IEEE Trans. Antennas Propag.*, vol. 64, no. 8, pp. 3692–3697, Aug. 2016.
[31] M. Ikram, N. Nguyen-Trong, and A. Abbosh, "Multiband MIMO microwave and millimeter antenna system employing dual-function tapered slot structure," *IEEE Trans. Antennas Propag.*, vol. 67, no. 8, pp. 5705–5710, Aug. 2019.
[32] Y. Liu, Y. Li, L. Ge, J. Wang, and B. Ai, "A compact hepta-band mode-composite antenna for sub (6, 28, and 38) GHz applications," *IEEE Trans. Antennas Propag.*, vol. 68, no. 4, pp. 2593–2602, Apr. 2020.
[33] R. Hussain, "Shared-aperture slot-based sub-6-GHz and mm-Wave IoT antenna for 5G applications," *IEEE Internet Things J.*, vol. 8, no. 13, pp. 10807–10814, Jul. 2021.
[34] S. Islam, M. Zada, and H. Yoo, "Low-pass filter based integrated 5G smartphone antenna for sub-6-GHz and mm-Wave bands," *IEEE Trans. Antennas Propag.*, vol. 69, no. 9, pp. 5424–5436, Sep. 2021.
[35] M. Wu and M. Chuang, "Multibroadband slotted bow-tie monopole antenna," *IEEE Antennas Wireless Propag. Lett.*, vol. 14, pp. 887–890, Apr. 2015.
[36] Y. Cao, Y. Cai, L. Wang, Z. Qian, and L. Zhu, "A review of substrate integrated waveguide end-fire antennas," *IEEE Access*, vol. 6, pp. 66243–66253, 2018.
[37] C. X. Mao, S. Gao, and Y. Wang, "Dual-band full-duplex Tx/Rx antennas for vehicular communications," *IEEE Trans. Veh. Technol.*, vol. 67, no. 5, pp. 4059–4070, May 2018.
[38] B. Feng, J. Chen, S. Yin, C. Y. D. Sim, and Z. Zhao, "A tri-polarized antenna with diverse radiation characteristics for 5G and V2X communications," *IEEE Trans. Veh. Technol.*, vol. 69, no. 9, pp. 10115–10126, Sep. 2020.
[39] J. K. Che, C. C. Chen, and J. F. Locke, "A compact four-channel MIMO 5G sub-6 GHz/LTE/WLAN/V2X antenna design for modern vehicles," *IEEE Trans. Antennas Propag.*, vol. 69, no. 11, pp. 7290–7297, Nov. 2021.
[40] A. Kiourti and K. S. Nikita, "Miniature scalp-implantable antennas for telemetry in the MICS and ISM bands: Design, safety considerations and link budget analysis," *IEEE Trans Antennas Propag.*, vol. 60, no. 8, pp. 3568–3575, Aug. 2012.
[41] J. Walfisch and H. L. Bertoni, "A theoretical model of UHF propagation in urban environments," *IEEE Trans Antennas Propag*, vol. 36, no. 12, pp. 1788–1796, Dec. 1988.
[42] "Minimum Detectable Signal Calculator." Everything RF. [Online]. Available: https://www.everythingrf.com/rf-calculators/minimum-detectable-signal-calculator (Accessed: Feb. 16, 2022).
[43] "V2X Functional and Performance Test Procedures—Selected Assessment of Device to Device Communication Aspects." 5G Automotive Association (5GAA). [Online]. Available: https://5gaa.org/wp-content/uploads/2018/10/5GAA_P-180092_TR_V2X_FP_Test_Procedures_v1.1.pdf (Accessed: Feb. 1, 2022).

Niamat Hussain (Member, IEEE) received the bachelor's degree in electronic engineering from the Dawood University of Engineering & Technology, Karachi, Pakistan, in 2014, the master's degree in electrical and computer engineering from Ajou University, Suwon, South Korea, in 2017, and the Ph.D. degree in information and communication engineering from Chungbuk National University (CBNU), Cheongju, South Korea, in 2021.

He worked as a Postdoctoral Researcher with CBNU from March 2021 to February 2022. He is currently working as an Assistant Professor with the Department of Smart Device Engineering, Sejong University, Seoul, South Korea. He has authored/coauthored more than 60 international journal papers. His research is mainly focused on 5G antennas, mm-wave antennas, terahertz antennas, wireless power transfer, and effects of electromagnetic effects on human health.

Dr. Hussain received the Best Paper Award in 2017 for his paper presented at the Korea Winter Conference (KIEES). He is also the recipient of the Outstanding Graduate Researcher Award and the Award of Merit in recognition of research achievements from the Dean of Graduate School, CBNU. In 2021, he was featured as World's Top 2% Scientists, ranked by the Standard University in collaboration with Elsevier. Moreover, he is a reviewer of many journals of IEEE, Elsevier, Wiley, and MDPI. He is also serving as a Guest Editor in a special issue (Prospective Multiple Antenna Technologies for 5G and Beyond) in Electronics.

Nam Kim received the B.S., M.S., and Ph.D. degrees in electronics engineering from Yonsei University, Seoul, South Korea, in 1981, 1983, and 1988, respectively.

He has been a Professor with the School of Information and Communication Engineering, Chungbuk National University, Cheongju, South Korea, since 1989. He has authored/coauthored more than 250 papers and has received almost 5000 citations. His research interests include optical information processing, health effect of EMF, wireless power transfer, and antennas for mobile communications.

Prof. Kim is a member of the International Advisory Committee for the World Health Organization Project on EMF, the IEEE International Committee on Electromagnetic Safety, and the International Electro Technical Commission TC 106. He was the President of the Bioelectromagnetics Society.